

## UNRAVELING THE HEMODYNAMIC IMPACT OF PERSISTENT ILIAC VEIN LESIONS AND PHYSICAL THERAPY POST-STENTING

ZHENMIN FAN<sup>1</sup>, JIAN LU<sup>1</sup>, ROBERT GUIDOIN<sup>2</sup>, XIAOYAN DENG<sup>1</sup>, XIA YE<sup>1,\*</sup>  
AND ZHIXIANG ZHANG<sup>3</sup> 

**Abstract.** Stent implantation is a standard treatment for iliac vein compression syndrome (IVCS), but persistent lesions in the stented vein can lead to adverse outcomes. This study investigates the hemodynamic impact of these lesions and the effects of therapeutic strategies post-stenting. A patient-specific model simulating flattened, narrow, and tissue adhesion (TA) lesions was used to analyze key hemodynamic parameters, including Wall Shear Stress (WSS), Oscillatory Shear Index (OSI), Relative Residence Time (RRT), and Flow Resistance (RF). The results show that contralateral venous lesions significantly worsen hemodynamic conditions in the iliac vein after stenting. The adhesion model exhibited significantly higher reflux volumes and more extensive regions of low TAWSS, high OSI, and high RRT compared to the other lesion models. Both active ankle exercises (AAE) and intermittent pneumatic compression (IPC) therapies improved the hemodynamic environment in the stented vein. However, these therapies also worsened blood flow disturbances at the contralateral lesion site. These findings highlight the importance of personalized therapeutic strategies to optimize clinical outcomes following stenting.

**Mathematics Subject Classification.** 76-XX, 76Zxx.

Received August 10, 2024. Accepted March 31, 2025.

### 1. INTRODUCTION

Iliac vein compression syndrome (IVCS), also known as May–Thurner syndrome (MTS), is typically caused by the persistent compression of the iliac arteries on the common iliac vein at the level of the fifth lumbar vertebra [1, 2]. Numerous studies have demonstrated that a significant proportion of IVCS patients experience obstruction of venous reflux in the lower limbs, leading to symptoms such as swelling, pigmentation, and venous ulcers [3, 4]. It has been reported that the incidence of lower extremity Deep vein thrombosis (DVT) due to IVCS ranges from 18% to 49%, predominantly affecting the elderly individuals and young women [5]. Clinical research indicates that iliac vein stent implantation is associated with minimal trauma and a higher long-term patency rate of the iliac vein, making it the preferred treatment for both thrombotic and non-thrombotic IVCS [6].

---

*Keywords and phrases:* Iliac vein compression syndrome, deep vein thrombus, stenting, hemodynamics, exercise, lesion.

<sup>1</sup> School of Mechanical Engineering, Jiangsu University of Technology, Changzhou Jiangsu 213001, China.

<sup>2</sup> Department of Surgery, Université Laval and Division of Regenerative Medicine, CHU de Québec Research Centre, Quebec, QC, Canada.

<sup>3</sup> Department of Neurology, The Second People’s Hospital of Changzhou, the Third Affiliated Hospital of Nanjing Medical University, Changzhou Medical Center of Nanjing Medical University. Changzhou 213003, China.

\* Corresponding author: [yx\\_laser0@163.com](mailto:yx_laser0@163.com)

However, follow-up studies have revealed that interventional therapy with iliac vein stents is accompanied by various complications, including an increased risk of DVT formation. These complications not only compromise stent patency but also significantly impede patient's recovery [7].

The hemodynamic environment after stent implantation is closely related to the formation of adverse clinical events. The formation of recirculation and stagnation flow caused by the protrusion of stent struts into the lumen significantly influences the spatial and temporal feature of blood flow [8–10]. This phenomenon is generally quantitatively analyzed by adverse wall shear stress (WSS), relative residence time (RRT), and oscillating shear stress index (OSI). It is posited that stent deployment in the host vein leads to unfavorable WSS, OSI, and RRT, which may increase the incidence of adverse clinical events post-stenting [11, 12]. Beyond the modifications instigated by stent placement on the host vessel, which subsequently modify the hemodynamic environment, the geometric attributes of the host vessel itself and the long-term post-procedural tissue remodeling caused by the intervention are also vital to the vascular blood flow environment [11]. Empirical evidence suggests that sites requiring stent implantation frequently exhibit a multitude of venous vascular pathologies [13]. Furthermore, clinical studies have identified a common association between iliac vein compression and multiple lesions [3–5]. While minor lesions generally do not necessitate intervention, their influence on hemodynamics should not be underestimated. Moreover, during the extended post-stenting phase, thrombosis of varying severity has been noted in the contralateral vessel, complicating the hemodynamics of the host vessel [8]. Notably, the sustained compression of the iliac vein, unlike arterial lesion sites, results in tissue adhesion. Studies have shown that most adhesions form near the junction of the right common iliac artery (RCIA) and left common iliac vein (LCIV). It is hypothesized that chronic pulsatile compression by the overlying RCIA leads to the development of “spurs” on the venous wall and partial venous obstruction [14]. Histological analysis shows that these spurs contain elastin, type I and III collagen, and smooth muscle cells [15]. According to the May–Thurner classification, approximately 21% of IVCS patients may develop tissue adhesions anywhere along the anterior and posterior aspects of the vein, causing the vein to be divided into two separate lumens [15]. Additionally, about 9% of patients experienced severe luminal occlusion, presenting as a porous, mesh-like structure in cross-section. Consequently, the post-implantation blood flow environment within the stent is strongly correlated with the lesion severity and stent implantation technique. These factors collectively contribute to thrombosis formation following stent implantation.

However, previous research has primarily focused on the effects of stent structure and intervention strategies on blood flow patterns, which have been shown to significantly influence hemodynamics [16–18]. Specifically, ‘S’-shaped stent struts offer enhanced flexibility, exerting minimal disruption to blood flow patterns. Increasing the stent spacing alleviates adverse flow effects, while new type stents have been shown to suppress chaos flow in contralateral blood flow. Following stent implantation at bifurcations, local flow velocity within the vessel decreases, and areas of low WSS are observed on the vessel wall [19]. Additionally, different intervention strategies can significantly influence the hemodynamic environment, with stent length in the inferior vena cava impacting the flow dynamics in the iliac vein and consequently altering the hemorheological properties of the contralateral vascular bifurcation [20, 21]. Although the impact of stents and stent implantation on the host vessel is crucial, the complexity of the implants, the presence of multifocal lower limb lesions, and the susceptibility of these regions to lower limb movements may lead to a markedly different hemodynamic environment following stent placement, compared to previous studies. Research has demonstrated the effectiveness of prevalent physical interventions, such as Active Ankle Exercise (AAE) and the utilization of Intermittent Pump Compression (IPC) devices, in the prevention of Deep Vein Thrombosis (DVT) [22]. Consequently, clinical guidelines generally advocate for the active participation in AAE in conjunction with IPC therapy during the rehabilitation process to optimally reduce the risk of thrombosis in the iliac-femoral veins [23, 24]. Consequently, this study develops a geometric model derived from the clinical imaging data of an elderly patient with Inferior Vena Cava Syndrome (IVCS), who received stent treatment for the left iliac vein. The study examines the influence of various lesions on the hemodynamic environment of the intervened iliac vein. Additionally, it explores the impact of common physical therapy on the altered hemodynamic environment of the intervened iliac vein.

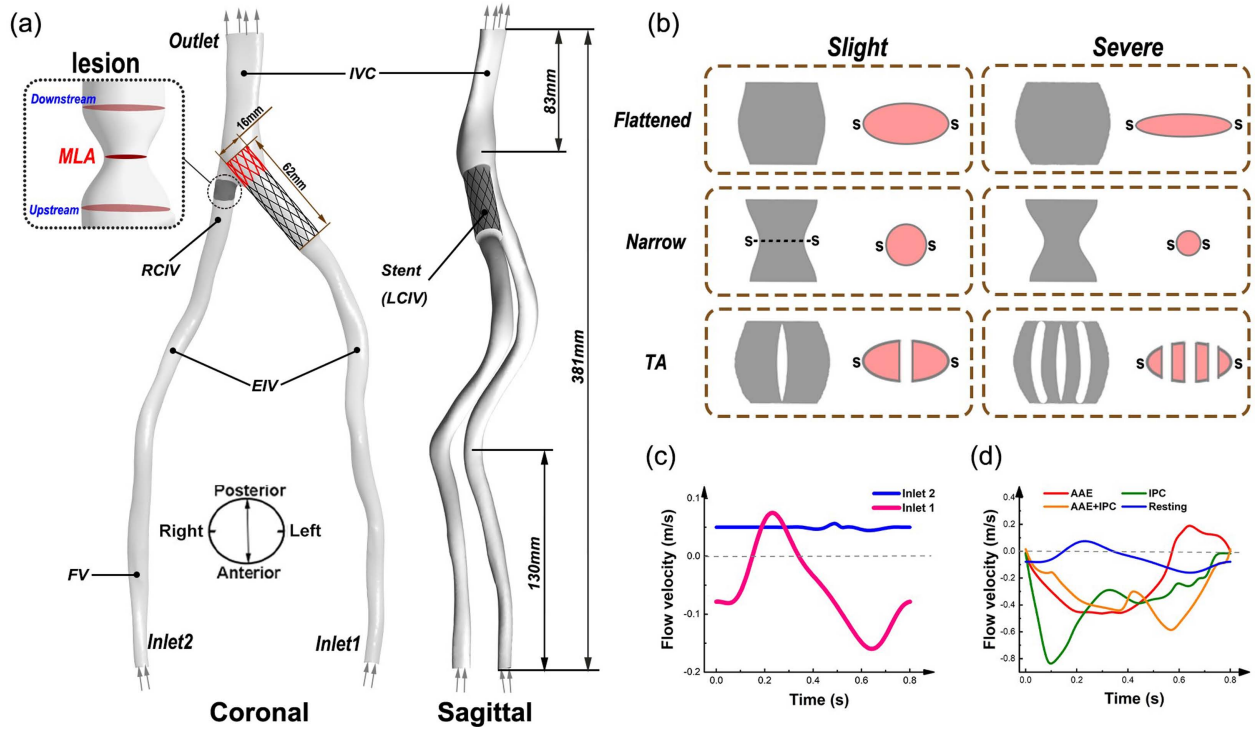


FIGURE 1. Iliac-femoral vein model. (a) The left iliac vein with an implanted stent. (b) Different types of lesions in the right iliac vein, which is the cross section at the minimum lumen area (MLA). (c) and (d) Flow velocity at the femoral vein inlet during resting and various types of physical therapies.

## 2. METHODS

### 2.1. Patient-specific model

A 65-year-old patient model with severe compression and deformation of the LCIV was obtained from The Second People's Hospital of Changzhou (file number: [2023] KY309-01, Changzhou, China). Lower extremity venography and computed tomography angiography (CTA) images were acquired using an imaging device (Siemens Medical Solution, Forchheim, Germany), with image dimensions of  $349 \times 349 \times 1217$  mm, a pixel size of 0.683 mm and a thickness of 1 mm per slice. After the patient signed an informed consent form, these data were collected and submitted to the local medical ethics committee. All procedures were conducted in accordance with the Helsinki Declaration.

Using the commercial software Minics 19.0 (Materialise, Plymouth, Michigan), the boundaries of the iliac vein bifurcation lumen were manually segmented. The initial model was subsequently refined using Geomagic 12.0 (Geomagic, North Carolina, USA), as shown in Figure 1. In this study, the widely utilized Wallstent was implanted, measuring 62 mm in length. It extended approximately 12 mm into the inferior vena cava to withstand compression from the iliac artery at the iliac vein bifurcation. The stent model was constructed along the lumen's centerline using SolidWorks 2020 (SolidWorks Corp, Concord, MA), excluding the left iliac compression area from the model. Each stent comprehensively covered the lesion site, boasting a diameter of 16 mm, thereby maintaining a lumen-to-stent diameter ratio of 1:1-1:1.2 [25].

To investigate the influence of various lesion types on patients with IVCS who have undergone stent implantation, we developed three distinct models of iliac lesions: **the flattened model**, which simulates the condition where both iliac veins are subjected to compression; **the narrow model**, which replicates the scenario of a

reduced cross-sectional area in the contralateral iliac vein; and **the spurs-like lesion model**, which emulates the adhesion of venous tissue following prolonged compression.

**The flattened model:** Based on the clinical characteristics of compressed vessels, the shape of the vessel is no longer circular, although its cross-sectional area remains unchanged [1, 2]. To simplify the model, the circumference at the lowest point of compression on the RCIV is assumed to remain consistent with its pre-compression state, and the cross-section at the compression site is approximated as an ideal ellipse. The configuration of each model's cross-section is governed by

$$\frac{x^2}{a^2} + \frac{y^2}{b^2} = 1 \quad (a > b > 0), \quad (2.1)$$

$$DRS = 1 - \frac{S_{post}}{S_{pre}}, \quad (2.2)$$

where  $x$  is the relative horizontal coordinate of the venous outer curve,  $y$  is the relative vertical coordinate ( $0 < x < a$ ,  $0 < y < b$ );  $a$  is the major axis of the lesion cross-sectional shape and  $b$  is the minor axis;  $S_{post}$  is the cross-sectional area of the lumen after iliac compression lesions,  $S_{pre}$  is the cross-sectional area of the lumen before iliac compression lesions.  $DRS$  is the stenosis rate of the flattening lesion.

**The narrow model:** This study adopted the definition of luminal stenosis by early work, where  $DRS'$  represents the percentage of reduction in the cross-sectional area of the venous lumen [26]:

$$DRS' = 1 - \left( \frac{R_{min}}{R_{max}} \right)^2 = 1 - (1 - \delta)^2, \quad (2.3)$$

where,  $R_{min}$  is the minimum diameter in the vein, and  $R_{max}$  is its maximum diameter. The equation for the peripheral curve at the stenosis site is as follows [27]:

$$r(x) = R_0 * \left( 1 - \frac{\delta}{2R_0} \left[ 1 + \cos \left( \frac{\pi x}{L} \right) \right] \right), \quad (2.4)$$

where,  $R_0$  is the radius of the vessel without stenosis, and  $r(x)$  is the radius of the vessel at point in  $x$ .  $\delta$  is the dimensionless radius,  $L$  is the length of the stenosis (defined here as 1.5 times the diameter of the CIA, approximately 15 mm), and  $x$  is the axial position of the radius within the stenosis ( $0 \leq x \leq L$ ).

**Tissue adhesion model:** The morphology of a spur has been reported to connect in a columnar fashion within the vein, leading to its classification as partially occluded [14, 28]. Figure 1b illustrates the tissue adhesion models employed in this study, which are generated under conditions of severe flattening. Each spur is represented as a uniformly shaped structure with a maximum cross-sectional thickness of approximately 1.5 mm.

## 2.2. Governing Equations

In this study, due to the extremely low velocity of blood flow in the vein, we assumed that all models were the laminar flow and the non-Newtonian rheological characteristics [29]:

$$\nabla \cdot u = 0, \quad (2.5)$$

$$\rho \left( \frac{\partial u}{\partial t} + u \cdot \nabla u \right) = -\nabla p + \nabla \cdot \tau, \quad (2.6)$$

$$\frac{\mu - \mu_\infty}{(\mu_0 - \mu_\infty)} = \left[ 1 + (\lambda \dot{\gamma})^2 \right]^{\frac{n-1}{2}}, \quad (2.7)$$

TABLE 1. The mesh independence study.

	Element	Nodes	$WSS_{max}$ (Pa)		$\Delta P$ (mmHg)	
	( $\times 10^4$ )	( $\times 10^4$ )	(Pa)	$Diff_1$ (%)	(mmHg)	$Diff_2$ (%)
1	152	21	1.495	–	1.365	–
2	204	40	1.830	18.31	1.507	9.42
3	301	57	1.982	7.66	1.48	1.82
4	518	78	2.04	2.93	1.492	0.81

where  $t$  is time,  $u$  is the velocity vector,  $p$  is pressure, and  $\rho$  (1060 kg/m<sup>3</sup>) is the density of blood [30].  $\mu_0$  (0.056 Pa·s) and  $\mu_\infty$  (0.00345 Pa·s) represent the dynamic viscosity of blood as the shear rate approaches zero and becomes large, respectively.  $\lambda$  and  $n$  are constants with values set to 3.313 s and 0.3568, respectively.

### 2.3. Boundary condition

For patients without right-side venous lesions, the inlet flow velocity was adopted from the healthy femoral vein inlet flow rate [31, 32], as shown in Figure 1c. In instances where lesions such as compression, narrowing, or tissue adhesion are present in the right CIV, a steady flow rate is discernible in the Doppler ultrasound waveform [31, 32]. Based on previous studies on the conditions of stenosis and diseased arterial outflow [33, 34], we allocate the inlet flow to the corresponding branches according to the degree of stenosis. The specific outflow distribution formula is as follows:

$$\begin{aligned} \frac{Q_{RCIA}}{Q_{LCIA}} &= -0.001x + 0.64, 0 \leq x \leq 64\% \\ \frac{Q_{RCIA}}{Q_{LCIA}} &= -0.015x + 1.57, x > 64\% \end{aligned} \quad (2.8)$$

where  $x$  represents the degree of stenosis, from which the outflow of the LCIA is calculated based on the healthy the femoral vein. The outflow of the CCA is obtained by subtracting the RCIA outflow from the total flow. Additionally, the flow velocities under resting conditions, after AAE, and after ICP are based on previous measurements of iliac vein flow velocity. The IVC outlet is set as an outflow boundary, with the outflow. Additionally, the vessel and stent walls are considered rigid, no-slip shear walls.

### 2.4. Calculation progress

In this study, the meshing of the iliac vein models was performed using ICEM-CFD (ANSYS, Inc, Canonsburg, USA) employing a combination of tetrahedral and hexahedral elements. To more accurately capture the low flow near the vein walls, a growth rate of 1.2 was used, with a total of five boundary layers, the first layer having a height of 0.1 mm. The mesh was locally refined at the junction between the stent, resulting in a maximum element size of 1 mm and a total element count ranging from approximately 2.40 to 3.01 million. After mesh independence testing, the maximum deviation in WSS and  $\Delta P$  values in the lesion areas among the models were found to be less than 5%, as shown in Table 1.

For  $WSS_{max}$ :

$$Diff_1 = \left| \frac{WSS_{max(i+1)} - WSS_{max(i)}}{WSS_{max(i)}} \right| * 100(\%) \quad (2.9)$$

For  $\Delta P$ :

$$Diff_2 = \left| \frac{\Delta P_{(i+1)} - \Delta P_{(i)}}{\Delta P_{(i)}} \right| * 100(\%). \quad (2.10)$$

This study was based on the finite element volume method and employs the CFD commercial software package ANSYS-Fluent 20.0 for numerical simulation. All models used the Simple algorithm, applying a second-order implicit Euler scheme for time discretization and a second-order upwind scheme for spatial discretization of the governing equations. Due to the unsteady nature of the pulsatile flow, each time step was required to converge to a residual standard of  $1 \times 10^{-5}$  to ensure precise data analysis. All results from the current simulation were obtained from the third cardiovascular cycle of the numerical computation.

## 2.5. Evaluation index

To quantitatively analyze the variations in hemodynamic conditions, this study examines the impact of three WSS-based hemodynamic parameters. Time-Averaged Wall Shear Stress (TAWSS), Oscillatory Shear Index (OSI), and Relative Residence Time (RRT) were described by [35]

$$\text{TAWSS} = \frac{1}{T} \int_0^T |\text{WSS}(s,t)| \cdot dt \quad (2.11)$$

$$\text{OSI} = \frac{1}{2} \left[ 1 - \left( \frac{|\int_0^T \text{WSS}(s,t) \cdot dt|}{\int_0^T |\text{WSS}(s,t)| dt} \right) \right] \quad (2.12)$$

$$\text{RRT} = \frac{1}{(1 - 2 \cdot \text{OSI}) \cdot \text{TAWSS}} \quad (2.13)$$

where  $T$  is the duration of the cardiac cycle,  $\text{WSS}$  is the instantaneous wall shear stress, and  $s$  represents the position the wall shear stress.

To more accurately capture the chaos blood flow within the lumen, we quantitative analyzed the flow in the direction opposite to the blood flow as reflux and quantify it using the reflux rate, which is expressed by

$$\text{Reflux rate} = \frac{V_w}{V_0} (\%), \quad (2.14)$$

where,  $V_w$  represents the volume of reflux flow and  $V_0$  represents the volume of blood flow.

Relative Flow Resistance (RF) was introduced to evaluate the venous patency [36]. The smaller the RF, the better the venous patency, and it was defined by

$$\text{RF} = \frac{\Delta P_1 - \Delta P_0}{\Delta P_0}, \quad (2.15)$$

where  $\Delta P_1$  represents the pressure drop along the diseased segment of the iliac vein from upstream to downstream of the lesion, and  $\Delta P_0$  represents the pressure drop along a non-diseased segment of the vein of the same length as  $\Delta P_1$ . The basic methodology of this work is commonly used in previous studies [37, 38].

## 3. RESULTS

### 3.1. Effect of lesions on the iliac vein

Figure 2 depicts the substantial disruption in flow observed at the juncture of a normal iliac vein model. In contrast to the healthy model, the lesion models of the iliac vein demonstrated an elevated flow velocity,

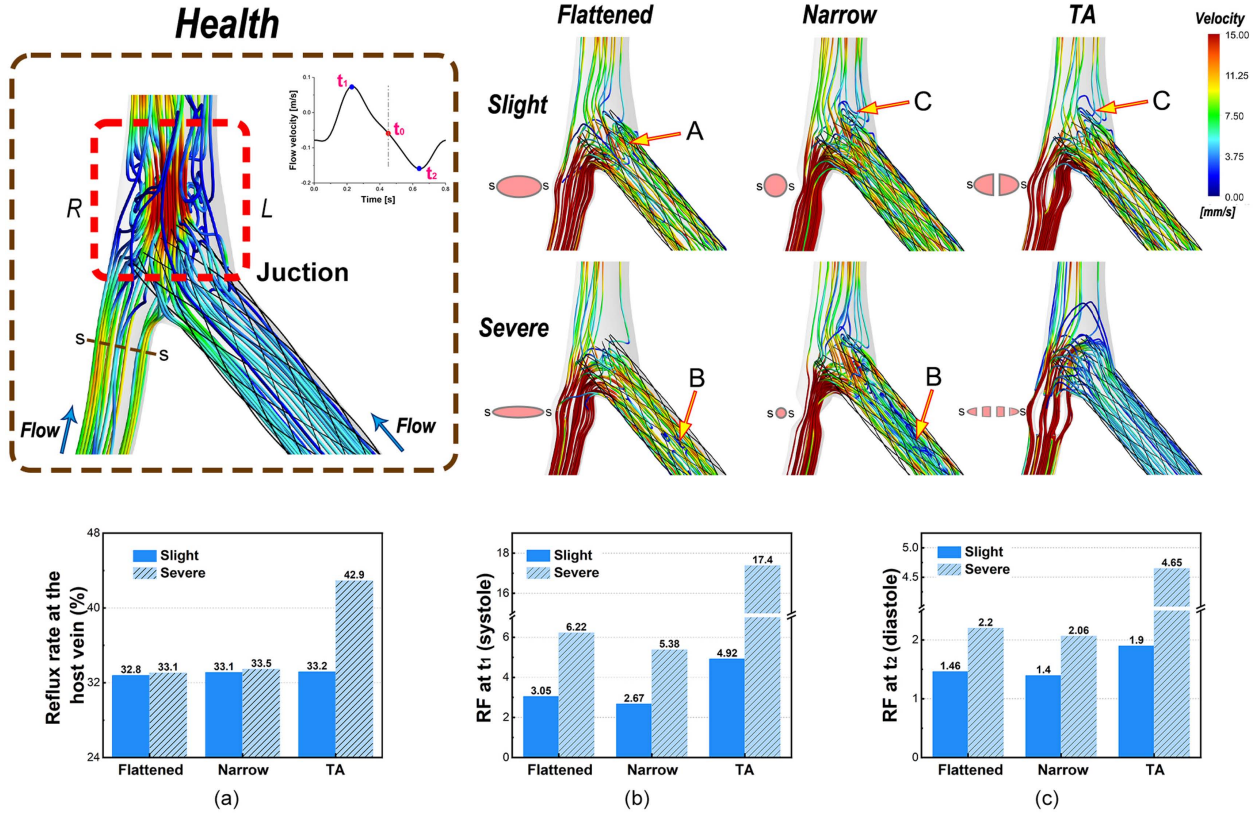


FIGURE 2. Effects of lesions on the right iliac vein after stenting. (a) Reflux rate of various lesion models in the host vessel at  $t_0$ . (b) Flow resistance (RF) at the lesion site at  $t_1$ . (c) Flow resistance (RF) at the lesion site at  $t_2$ .

which mitigated the disturbed flow at the lesion site to a certain degree and enhanced the blood flow in the vicinity of the junction. In the flattened model, there are more low-velocity regions on the left side of the iliac vein near the bifurcation (region C), a phenomenon that becomes more pronounced in models with more severe compression. The flattened model, however, differs. The flow lines in the iliac vein are relatively parallel to the vessel lumen, but more chaos regions appear at the stent's distal end. As the degree of stenosis increases, higher flow velocities are observed in some areas, and in severe models, localized low-velocity regions develop at the stent segment (region B). In the tissue adhesion model, the flow velocity distribution in the iliac vein is highly uneven, with a marked reduction in flow velocity at the stent segment in more severe models. Meanwhile, disturbed low-velocity regions appear at both the distal end of the stent and in the iliac vein.

The results of the quantitative analysis reveal that the lesion models demonstrated the reflux volume at the time point  $t_0$ . The models characterized by flattening and narrowness displayed comparable reflux rates. However, the adhesion model demonstrated a reflux rate that was markedly higher than the rates observed in the other two types of lesions. This discrepancy became increasingly pronounced as the degree of compression escalated. Further analysis revealed that the increased severity of the lesions (the flattened model the narrow model and the tissue adhesion model) led to greater resistance within the models. The RF in the vein model with adhesions reached a maximum, being at least 1.3 times higher during the systolic period and 1.84 times higher during the diastolic period compared to the other models. Additionally, RF during the diastolic period was significantly greater than during the systolic period in the iliac vein's cardiac cycle. Therefore, the increase in lesion severity leads to higher flow resistance within the host vein.

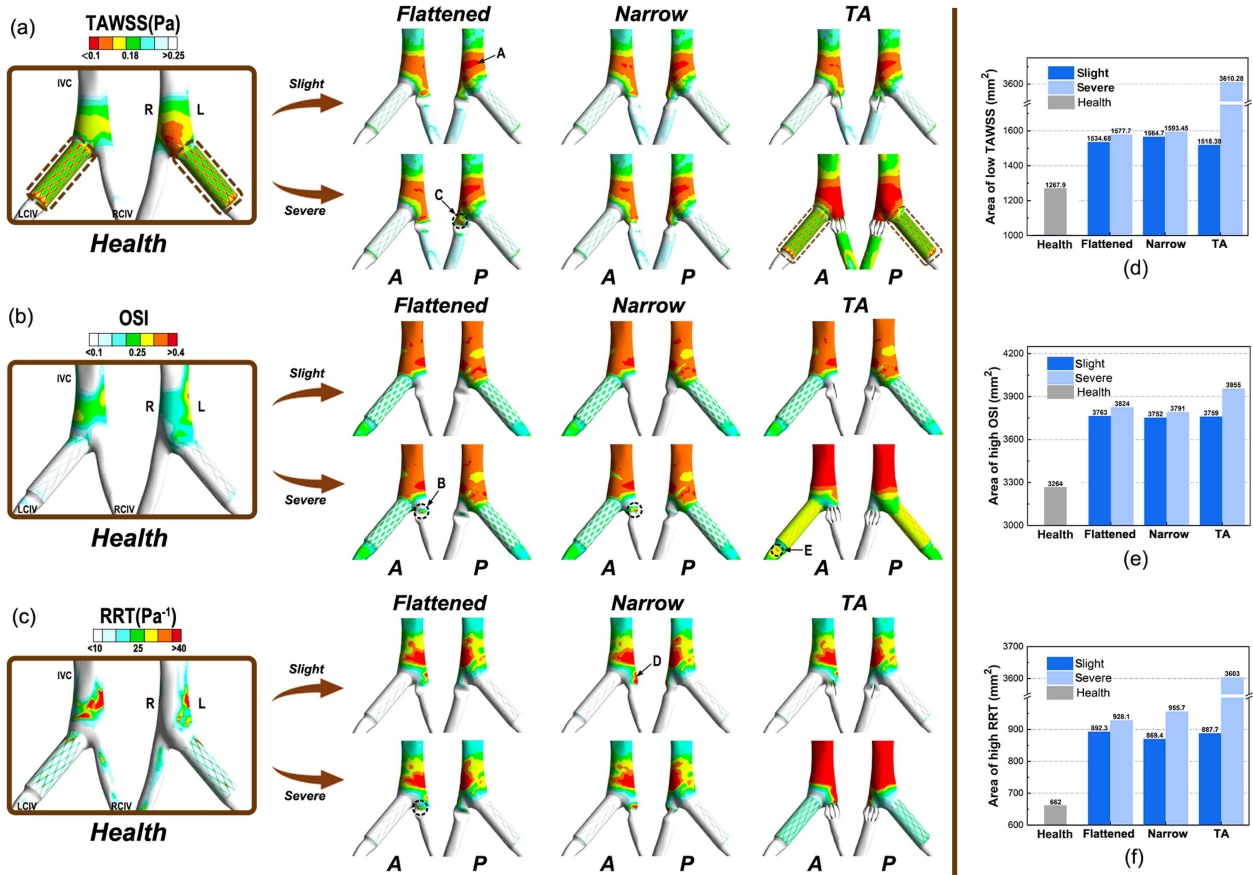


FIGURE 3. (a–c) Distribution of TAWSS, OSI, and RRT after iliac vein stenting. (d–f) Quantitative analysis of adverse hemodynamic parameters in iliac-femoral vein model.

In all the venous lesion models depicted in Figure 3, the regions with low TAWSS, high OSI, and high RRT were significantly larger in comparison to the healthy vein model. Significant expanses of low TAWSS are observed in healthy veins, specifically in areas proximal to the stent struts and the posterior wall at the junction of the iliac vein, designated as region A. Following the occurrence of a lesion, there is a notable increase in regions of low TAWSS, high OSI, and high RRT across all models, with a particular emphasis on the anterior and posterior walls at the junction. Among the models, the model exhibiting tissue adhesion presented the most extensive areas of low TAWSS, high OSI, and high RRT.

Moreover, as lesion severity increased, all lesion types- the flattened model, the narrow model, and the tissue adhesion model- exhibited worsening blood flow.

In order to more comprehensively assess the influence of unfavorable hemodynamic factors on the host venous wall, we undertook a quantitative statistical analysis of these factors by area, as shown in Figures 3d–3f. It is clear from the model of the iliac vein without a lesion that the areas with low TAWSS, high OSI, and high RRT were minimal. Furthermore, these areas expanded in correlation with the severity of the lesion across the three disease models. Notably, the model with severe tissue adhesion demonstrated the most extensive adverse hemodynamic impacts. Specifically, the areas with low WSS, high OSI, and high RRT in the model were approximately 2.26, 1.03, and 3.77 times larger, respectively, compared to those in the other lesion models.

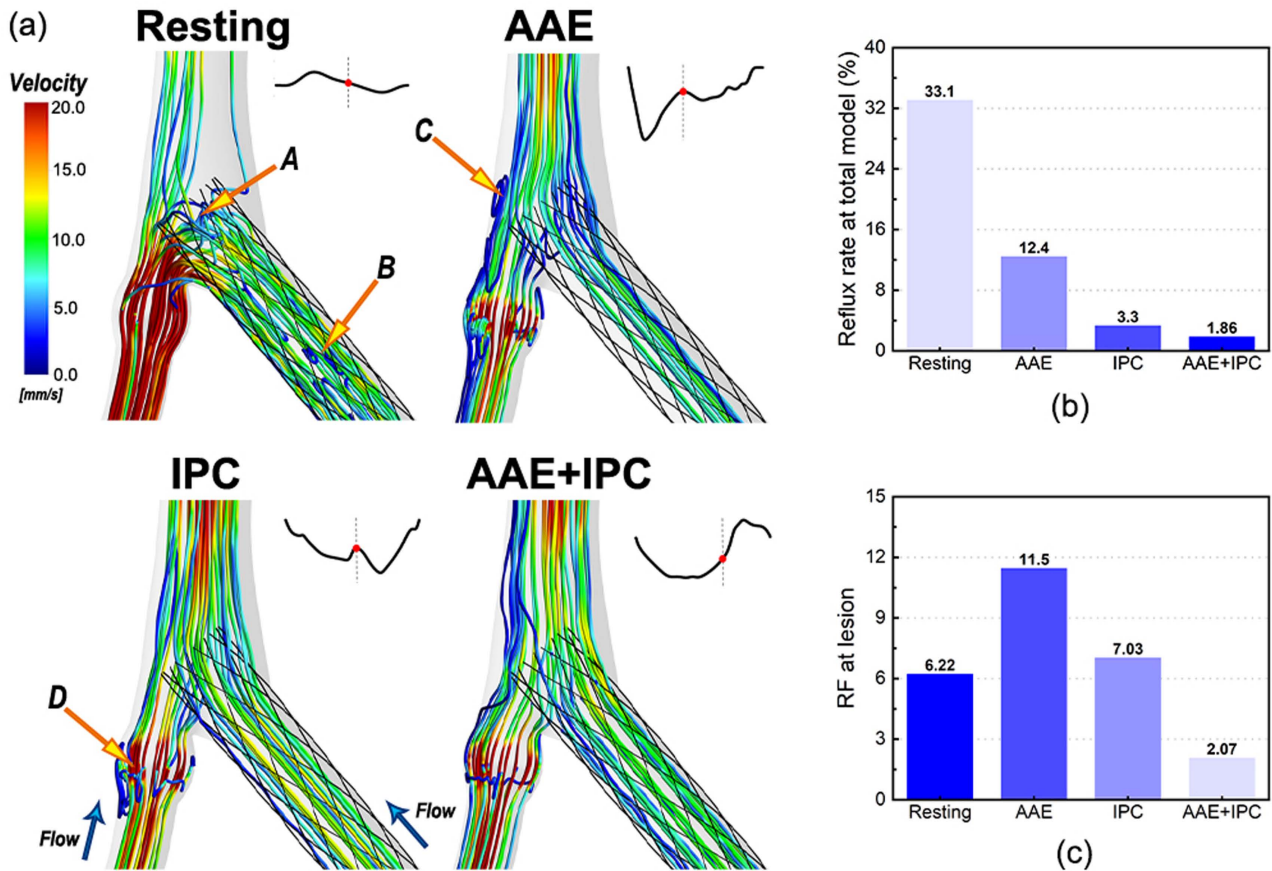


FIGURE 4. Effects of physical therapy on the hemodynamic environment after iliac vein stenting. (a) Streamlines of the model at physical therapies at different time. (b) Quantitative analysis of adverse hemodynamic parameters after different physical therapies. (c) Flow resistance at the lesion site. (Note: Resting, AAE, IPC and AAE+IPC represent the iliac vein model under the conditions of resting state, AAE activity alone, IPC therapy alone and AAE and IPC combined therapy, respectively).

### 3.2. Effect of physical therapy on the host iliac vein

As depicted in Figure 4, the influence of three prevalent physical therapies on blood circulation post-iliac vein stenting in subjects with lesions is examined. Each of the three treatments enhanced the flow velocity in the vicinity of the stent on the confluence side. Although the impact of AAE activity in isolation is marginally less effective, primarily resulting in low-velocity disturbed flow, which is mainly located at the stent's proximal end, the most significant improvement is observed under IPC therapy and the combined therapy of AAE and IPC. However, all three external interventions resulted in disrupted flow at the lesion site. Despite the quantitative evidence suggesting a significant reduction in post-treatment reflux volume, particularly under the combined therapy of AAE and IPC, the Resting model still demonstrated the highest reflux flow, approximately 2.67 times higher than that of other therapeutic interventions. Interestingly, the combined therapy model of AAE and IPC showed negligible significant reflux.

Figure 5 illustrates notable variances in the distribution of TAWSS, OSI, and RRT on the surface of the iliac vein wall under varying physical therapies. The region of low WSS in the Resting model is the most obvious, even extending downstream to the outer wall of the lesion. However, post-treatment, a marked increase in overall

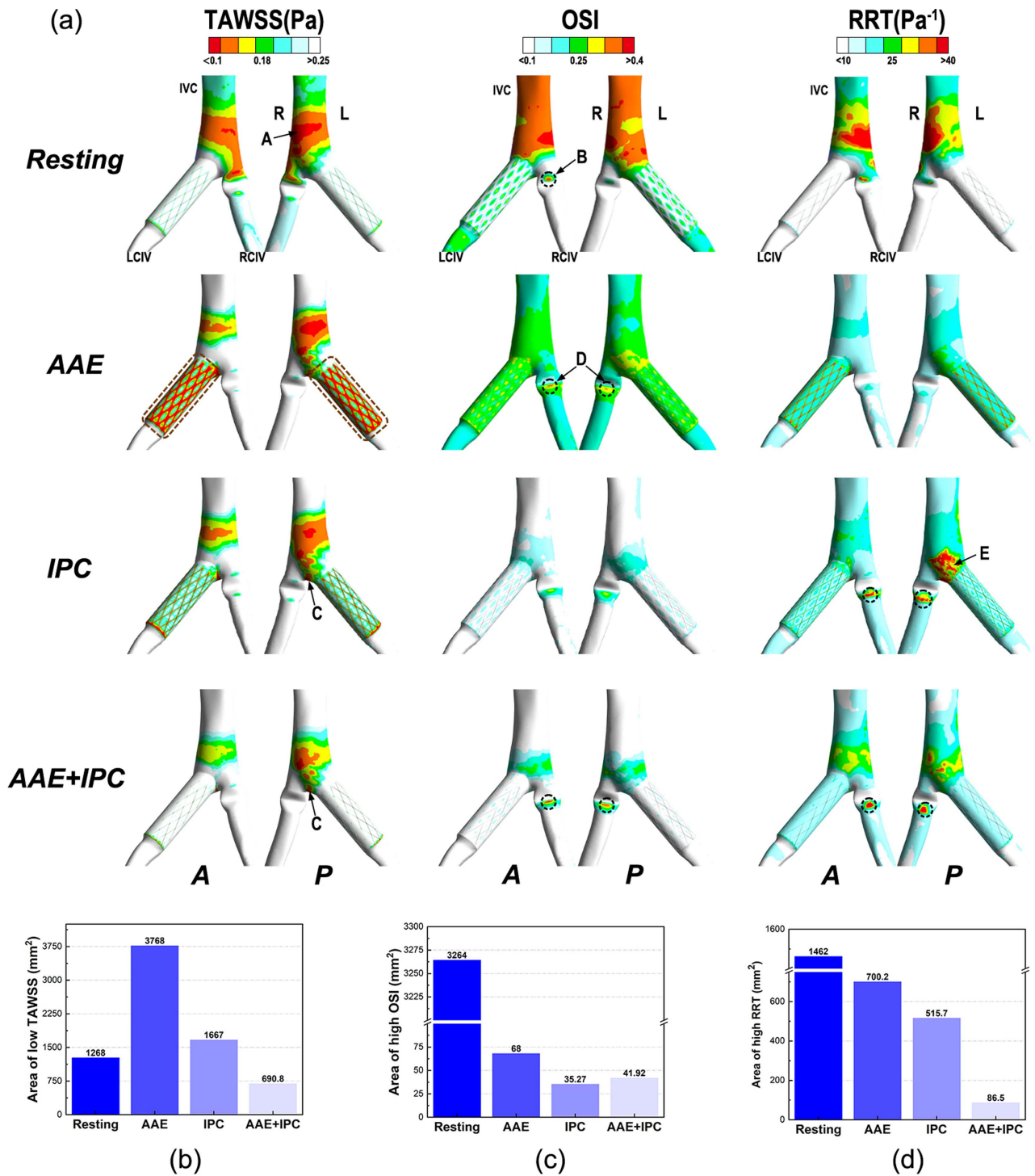


FIGURE 5. (a) Distribution of TAWSS, OSI and RRT after different physical therapies for the stented iliac vein. (b–d) Quantitative analysis of adverse hemodynamic parameters after different physical therapies.

shear stress occurs, along with a corresponding decrease in the low WSS area. Moreover, both IPC-treated vein models demonstrate a significant reduction in the low WSS region at the junction. This phenomenon is even more pronounced in the distribution of OSI and RRT. In the host vein model treated with IPC, which combines both AAE and IPC exercises, the regions with high OSI and RRT were significantly reduced. An in-depth quantitative analysis of the dispersion of adverse hemodynamic parameters under different physical therapies was performed, as depicted in Figure 5b–5d. The findings indicated that the area of high OSI is maximized when the host is at rest, approximately 48 times larger than in other models. IPC can significantly reduce RRT values, particularly when combined with AAE.

#### 4. DISCUSSION

Currently, the implantation of a stent in the lower limb vein is widely recognized as a standard therapeutic intervention for pathological obstructions or stenoses in the deep venous system. Nonetheless, interventional therapy continues to encounter numerous clinical obstacles, with postoperative thrombosis emerging as a relatively frequent complication [10]. This study examines the effect of lesions in the right iliac vein following stent implantation on blood flow. Furthermore, it explores the impact of lower limb rehabilitation therapy on enhancing the blood flow environment within the host vein.

The present study identified three specific lesion types in the right iliac vein - namely, the flattened vein, the narrow vein, and the tissue adhesion vein- have the potential to instigate detrimental local hemodynamic environments, characterized by reflux flow, flow resistance, low WSS, high OSI, and RRT. It was observed that the severity of these adverse conditions escalated with the increasing severity of the lesions. These unfavorable hemodynamic characteristics may be closely related to the incidence of adverse events following stent implantation at this location, which could significantly explain for the suboptimal clinical outcomes observed post-stenting [39]. The intricate spatial arrangement of the iliac and vena cava bifurcation vessels requires consideration of numerous factors in managing the hemodynamic environment post-stenting. Consequently, the clinical outcome following iliac vein stenting is not solely dependent on the blood flow environment within the stent segment, but also significantly influenced by the contralateral vessel [10, 40]. The findings of this study suggest that during the execution of interventional treatment on the iliac vein, careful consideration must be given to the state of the contralateral vessel to attain superior clinical results. Proactive interventions are imperative, particularly in instances of tissue adhesion, pronounced compression, and substantial stenosis.

This research further revealed that the use of physical therapies, including AAE and IPC, on sedentary patients can notably enhance the aberrant hemodynamic properties of the iliac vein wall. The simulation outcomes suggested that these physical therapies can substantially alleviate detrimental blood flow post-stent implantation by augmenting blood circulation compared to resting state.

This significant augmentation in blood flow rate could potentially be associated with the effect of diminishing venous blood stagnation, which might be a crucial factor contributing to the positive clinical results observed with these therapeutic interventions [40–42]. Nonetheless, our research also found that these rehabilitation treatments may not yield beneficial results for patients with lesions on the contralateral side. The study indicates that rehabilitation treatments could exacerbate conditions for patients with multiple diseases in the contralateral vein, due to the significant emergence of more disturbed flow regions (low TAWSS, high OSI, and RRT), thereby potentially triggering or enhancing stent-restenosis or stent thrombosis. Consequently, these factors could be the key contributors to the adverse clinical responses observed in relation to these treatments. This implies that post-intervention, the patient may be susceptible to multiple complications due to significant alterations in local blood flow. Consequently, physical therapies may exhibit beneficial therapeutic impacts on healthy populations such as AAE and IPC therapy. However, individuals with multiple lesions must be cautious. Our hypothesis posits that patients with multiple lesions in the contralateral vein may not be ideal candidates for physical treatment. These findings further suggest that rehabilitative training for patients' post-intervention should only be undertaken after a thorough assessment of vascular function.

While this research provides valuable insights into alterations in the blood flow environment within the host iliac vein following stent implantation, thereby offering some clinical surgical references, the generalizability of

the conclusions is limited due to the study's reliance on a single case. Moreover, in this study, we simplified the influence of exercise and external stimuli to changes in flow velocity, which is reasonable given the substantial variations in flow velocity under different conditions. Future investigations could potentially enhance the applicability of these findings by incorporating a wider range of locations and combining in vitro testing [19, 43], thereby more accurately reflecting the physiological environment of IVCS post-stent implantation in the host vein.

## 5. CONCLUSION

The implantation of an iliac vein stent is a widely accepted treatment for IVCS, though it may result in adverse events post-intervention. This study investigates the impact of persistent iliac vein lesions on the hemodynamic environment following stent implantation. The numerical data indicate that contralateral venous lesions, such as flattened, narrow, and tissue adhesion lesions, exacerbate the hemodynamic conditions in the iliac vein post-stenting. The findings show that lesion models demonstrate higher flow velocities, which reduce flow disturbance at the lesion site, but lead to localized low-velocity regions upstream and downstream of the lesion, especially as stenosis severity increases. Furthermore, the adhesion model exhibited significantly higher reflux volumes and adverse hemodynamic conditions, with larger regions of low TAWSS, high OSI, and high RRT compared to the flattened and narrow models. Additionally, the results indicate that both AAE and IPC therapies significantly improve the hemodynamic conditions near the stent segment. While AAE activity alone has a marginal effect on the overall hemodynamic environment, IPC therapy and the combined AAE-IPC therapy yield the best results. Despite these improvements, these therapies may unintentionally create an unfavorable blood flow environment at the contralateral lesion site, potentially exacerbating the lesion.

## ACKNOWLEDGMENTS

This work is supported by National Natural Science Research Foundation of China (No. 12372305, 12272153, 12202274, 11902126), Changzhou Science and Technology Support Program (Changzhou Science and Technology Support Program (CJ20241077), the Clinical Research Project of Changzhou Medical Center of Nanjing Medical University (CMCC202304) and Outstanding young backbone teacher of Jiangsu Qinglan Project, Zhongwu young innovative talents projection from Jiangsu Institute of Technology.

## CONFLICTS OF INTEREST

All authors declare no competing interests.

## DATA AVAILABILITY STATEMENT

No new data/codes were created or analyzed in this study.

## REFERENCES

- [1] K.N. Brinegar, *et al.*, Iliac Vein Compression Syndrome: Clinical, Imaging and Pathologic Findings. *World J. Radiol.* **7** (2015) 375.
- [2] S. Butros, *et al.*, Venous compression syndromes: clinical features, imaging findings and management. *Br. J. Radiol.* **86** (2013) 20130284.
- [3] Z. Liu, *et al.*, Endovascular treatment for symptomatic iliac vein compression syndrome: a prospective consecutive series of 48 patients. *Ann. Vasc. Surg.* **28** (2014) 695–704.
- [4] Q. Radaideh, N.M. Patel and N.W. Shammas, Iliac vein compression: epidemiology, diagnosis and treatment. *Vasc. Health Risk Manage.* (2019) 115–122.
- [5] Z. Liu, *et al.*, Endovascular treatment for symptomatic iliac vein compression syndrome: a prospective consecutive series of 48 patients. *Ann. Vasc. Surg.* **28** (2014) 695–704.
- [6] A.K. Stuck, *et al.*, Patency and clinical outcomes of a dedicated, self-expanding, hybrid oblique stent used in the treatment of common iliac vein compression. *J. Endovasc. Ther.* **24** (2017) 159–166.

- [7] H. Wang, *et al.*, A systematic review of DVT and stent restenosis after stent implantation for iliac vein compression syndrome. *Med. Novel Technol. Devices* **15** (2022) 100125.
- [8] C. Li, *et al.*, The influencing mechanism of iliac vein stent implantation for hemodynamics at the bifurcation. *Comput. Methods Biomech. Biomed. Engin.* **26** (2023) 1452–1461.
- [9] C. Peng, *et al.*, Numerical simulation in the abdominal aorta and the visceral arteries with or without stenosis based on 2D PCMRI. *Int. J. Numer. Method Biomed. Eng.* **38** (2022) e3569.
- [10] T.B. Le, *et al.*, Contralateral deep vein thrombosis after iliac vein stent placement in patients with May–Thurner syndrome. *J. Vasc. Interv. Radiol.* **29** (2018) 774–780.
- [11] J.K. Chesnutt, H.-C.J.C.i.b. Han, and Medicine, Simulation of the microscopic process during initiation of stent thrombosis. *Comput. Biol. Med.* **56** (2015) 182–191.
- [12] T. Inoue, *et al.*, Vascular inflammation and repair: implications for re-endothelialization, restenosis, and stent thrombosis. *JACC Cardiovasc. Interv.* **4** (2011) 1057–1066.
- [13] B.E. Claessen, *et al.*, Stent thrombosis: a clinical perspective. *JACC Cardiovasc. Interv.* **7** (2014) 1081–1092.
- [14] R. May and J.J.A. Thurner, The cause of the predominantly sinistral occurrence of thrombosis of the pelvic veins. *Angiology* **8** (1957) 419–427.
- [15] A. Esposito, *et al.*, A comprehensive review of the pathophysiology and clinical importance of iliac vein obstruction. **60** (2020) 118–125.
- [16] C. Shen, *et al.*, Secondary flow in bifurcations - Important effects of curvature, bifurcation angle and stents. *J. Biomech.* **129** (2021) 110755.
- [17] K. Mori and T. Saito, Effects of stent structure on stent flexibility measurements. *Ann. Biomed. Eng.* **33** (2005) 733–742.
- [18] C. Huang, *et al.*, Fusion of optical coherence tomography and angiography for numerical simulation of hemodynamics in bioresorbable stented coronary artery based on patient-specific model. *Comput. Assist. Surg. (Abingdon)* **22** (2017) 127–134.
- [19] J.M. Hu, *et al.*, Mechanism of effect of stenting on hemodynamics at iliac vein bifurcation. *Comput. Biol. Med.* **170** (2024).
- [20] J. Hu, *et al.*, Mechanism of effect of stenting on hemodynamics at iliac vein bifurcation. *Comput. Biol. Med.* **170** (2024) 107968.
- [21] Z. Fan, *et al.*, Insights from computational fluid dynamics and in vitro studies for stent protrusion in iliac vein: how far shall we go? *Cardiovasc. Eng. Technol.* (2024).
- [22] K. Vowden, The use of intermittent pneumatic compression in venous ulceration. *Br. J. Nurs.* **10** (2001) 491–509.
- [23] K. Sakai, *et al.*, Effects of intermittent pneumatic compression on femoral vein peak venous velocity during active ankle exercise. *J. Orthop. Surg.* **29** (2021) 2309499021998105.
- [24] P. Lachiewicz, S. Kelley and L. Haden, Two mechanical devices for prophylaxis of thromboembolism after total knee arthroplasty: a prospective, randomised study. *J. Bone Joint Surg. Br.* **86** (2004) 1137–1141.
- [25] S. Raju, P. Tackett Jr. and P. Neglen, Reinterventions for nonocclusive iliofemoral venous stent malfunctions. *J. Vasc. Surg.* **49** (2009) 511–518.
- [26] L. Ai, K.J.I.j.o.h. Vafai, and M. Transfer, A coupling model for macromolecule transport in a stenosed arterial wall. *Int. J. Heat. Mass. Tran.* **49** (2006) 1568–1591.
- [27] I. Di Venuta, A. Boghi and F. Gori, Three-dimensional numerical simulation of a failed coronary stent implant at different degrees of residual stenosis. Part I: fluid dynamics and shear stress on the vascular wall. *Numer. Heat Transfer A: Appl.* **71** (2017) 638–652.
- [28] C.M. Murtha, *et al.*, A cadaver study evaluating intraluminal anomalies of the left common iliac vein. *J. Vasc. Surg. Venous Lymphat. Disord.* (2024) 101837.
- [29] U. Morbiducci, *et al.*, On the importance of blood rheology for bulk flow in hemodynamic models of the carotid bifurcation. *J. Biomech.* **44** (2011) 2427–2438.
- [30] U. Morbiducci, *et al.*, Quantitative analysis of bulk flow in image-based hemodynamic models of the carotid bifurcation: the influence of outflow conditions as test case. *Ann. Biomed. Eng.* **38** (2010) 3688–3705.
- [31] E.P. Lin, *et al.*, The importance of monophasic Doppler waveforms in the common femoral vein: a retrospective study. *J/ Ultrasound Med.* **26** (2007) 885–891.
- [32] E.P. Lin, S. Bhatt and V.S.J.U.C. Dogra, Lower extremity venous Doppler. **3** (2008) 147–158.

- [33] L. Changsheng, *et al.*, Influence of the anatomical structure on the hemodynamics of iliac vein stenosis. *J. Biomech. Eng.* **145** (2023) 011013.
- [34] K.M. Saqr, *et al.*, Evidence for non-Newtonian behavior of intracranial blood flow from Doppler ultrasonography measurements. *Med. Biol. Eng. Comput.* **57** (2019) 1029–1036.
- [35] X. Zhang, *et al.*, Hemodynamic impact of snoring on carotid artery after stent implantation: the role of oscillation. *Acta Bioeng. Biomech.* **25** (2023).
- [36] S. Zhang, *et al.*, CFD Study on Hemodynamic Characteristics of Inferior Vena Cava Filter Affected by Blood Vessel Diameter. Tech Science Press (2023).
- [37] C.Q. Li, *et al.*, Effect of stent treatment on hemodynamics in iliac vein compression syndrome with collateral vein. *Med. Eng. Phys.* **115** (2023).
- [38] H.W. Chen, *et al.*, CFD Study of the Effect of the Angle Pattern on Iliac Vein Compression Syndrome. *Bioengineering-Basel* **10** (2023).
- [39] U. Morbiducci, *et al.*, Outflow conditions for image-based hemodynamic models of the carotid bifurcation: implications for indicators of abnormal flow. *J. Biomech. Eng.* (2010).
- [40] A., I.Z. *et al.*, Anultrasound imaging and computational fluid dynamics protocol to assess hemodynamics in iliac vein compression syndrome. *J. Vasc. Surg. Venous Lymph. Disord.* **11** (2023) 1023–1033.
- [41] K.J.B.J.o.N. Vowden, The use of intermittent pneumatic compression in venous ulceration. *Br. J. Nurs.* **10** (2001) 491–509.
- [42] K. Sakai, *et al.*, A novel device for lower leg intermittent pneumatic compression synchronized with active ankle exercise for prevention of deep vein thrombosis. *Phlebology* **37** (2022) 507–515.
- [43] Z.M. Fan, *et al.*, Insights from computational fluid dynamics and in vitro studies for stent protrusion in iliac vein: how far shall we go? *Cardiovasc. Eng. Technol.* (2024).



**Please help to maintain this journal in open access!**

This journal is currently published in open access under the Subscribe to Open model (S2O). We are thankful to our subscribers and supporters for making it possible to publish this journal in open access in the current year, free of charge for authors and readers.

Check with your library that it subscribes to the journal, or consider making a personal donation to the S2O programme by contacting [subscribers@edpsciences.org](mailto:subscribers@edpsciences.org).

More information, including a list of supporters and financial transparency reports, is available at <https://edpsciences.org/en/subscribe-to-open-s2o>.